Research Article

One-Pot Synthesis of Magnetic Polypyrrole Nanotubes for Adsorption of Cr(VI) in Aqueous Solution

Wenjuan Zhang [ID] **,[1,2] Yaxian Wang,[2] Yulong Fei,[2] Youliang Wang,[3] Zhaoxiong Zhang,[2] Miao Kou,[2] Qiancheng Feng,[2] Sheng Wang,[1,2] and Xueyan Du[1,2]**

[1]*State Key Laboratory of Advanced Processing and Recycling of Non-Ferrous Metals, Lanzhou University of Technology, Lanzhou 730050, China*
[2]*School of Materials Science and Engineering, Lanzhou University of Technology, Lanzhou 730050, China*
[3]*School of Mechanical and Electrical Engineering, Lanzhou University of Technology, Lanzhou 730050, China*

Correspondence should be addressed to Wenjuan Zhang; wenjuanzhang86@163.com

A novel and efficient route is proposed to fabricate Fe_3O_4/polypyrrole (Fe_3O_4/PPy) nanotubes via a one-pot process. The one-pot strategy involves the synthesis of Fe_3O_4/PPy nanotubes by oxidative polymerization of pyrrole (Py) monomer using Fe^{3+} as an oxidant in the presence of methyl orange (MO) and Fe^{3+} used as iron source to form Fe_3O_4 simultaneously in basic conditions without adding any additional iron source and oxidant. The effects of Fe^{3+} concentration on the morphology and adsorption capacity of the Fe_3O_4/PPy nanotubes were investigated. The Fe_3O_4/PPy nanotubes exhibit a tubular structure. Fe_3O_4 nanoparticles are well dispersed among the PPy nanotubes. The Fe_3O_4/PPy nanotubes exhibit excellent magnetic property, which make them easy to separate from wastewater by magnetic separation. The diameter of the PPy nanotubes decreased with the increase of the Fe^{3+} concentration. The Fe_3O_4/PPy nanotubes showed strong adsorption capability for Cr(VI) with the maximum adsorption capacity of about 451.45 $mg·g^{-1}$, which is significantly higher than bare Fe_3O_4 nanoparticles. Cr(VI) was adsorbed on Fe_3O_4/PPy nanotubes by ion exchange and chelation, where Cr(VI) was partially reduced to Cr(III) due to the existence of $-NH^+$ on the Fe_3O_4/PPy nanotubes. Furthermore, the Fe_3O_4/PPy nanotubes are recyclable, retaining 90% of the initial removal efficiency after 5 adsorption/desorption cycles.

1. Introduction

With the rapid development of industry, water pollution is increasingly becoming a ubiquitous environmental problem. The pollution of toxic dyes and heavy metal ions exists widely because they are commonly used in or generated by a number of industrial processes. Among them, the heavy metal ion Cr(VI) was considered to be a major pollutant because it is widely applied in chromium plating, textile industries, photography, and printing inks [1, 2]. In addition, Cr(VI) has the high toxicity and tends to bioaccumulate in the human body through the food chain, causing great damage to humans and other organisms. Therefore, the recommended maximum allowable concentrations of

Cr(VI) in domestic water supply and inland surface water are, respectively, 0.05 mg/L and 0.1 mg/L [3, 4]. At present, many methods have been used to reduce/remove Cr(VI) from aqueous solution, such as adsorption method, precipitation method, and membrane separation method [5]. Among them, the adsorption technology has been extensively studied due to its economic feasibility and high removal ability of toxic heavy metals and other pollutants [6].

Magnetic nanoparticles (MNPs) have attracted much attention to remove harmful heavy metal ions from wastewater because they have high adsorption capacity, high specific surface area, easy separation and regeneration, and surface functional group modification [7–9]. Furthermore, MNPs have outstanding magnetic properties and can be

magnetically separated from solution using a magnet [10]. However, MNPs tend to agglomerate and have poor thermodynamic stability due to their high surface energy [11, 12]. These reduced reactivity sites and the specific surface area of MNPs, which will further influence the removal of heavy metal ions by MNPs. At present, coating MNPs using functional polymers can improve properties of MNPs, in particular, conductive polymers [13] (e.g., polypyrrole, polythiophene, and polyaniline). Of conducting polymers, PPy was the most studied conductive polymer due to the excellent stability in the environment [14] and good removal capacity of heavy metal [15, 16]. The coating of PPy can avoid agglomeration and oxidation of MNPs. Furthermore, PPy has good adsorption properties for Cr(VI) from wastewater owing to their rich functional groups and environmental stability [17–19].

At present, preparation and application of magnetic PPy composites in removal of heavy metal have been reported. For example, Chávez-Guajardo et al. [20] first prepared the maghemite nanoparticles using chemical coprecipitation methods. Subsequently, they synthesized the PPy/γ-Fe$_2$O$_3$ (MNCs) through emulsion polymerization of pyrrole. MNCs were used as active agents for removing Cr(VI) and Cu(II), which showed adsorption capacity of 209 mg·g^{-1} for Cr(VI). Other researchers have prepared Fe$_3$O$_4$/PPy microspheres by similar methods, the Fe$_3$O$_4$ particles played the role of "seeds" in composite microspheres, and the PPy was used as the "pulp and peel" to form "core-shell" structure. When used as an absorbent of heavy ions, Fe$_3$O$_4$/PPy microspheres exhibit the maximum adsorption capacity for Ag(I) of 143.3 mg·g^{-1} [21] and Cr(VI) removal of 238.1 mg·g^{-1} [22]. The adsorption capacity needs to be further improved. Therefore, in order to further improve the adsorption capacity of magnetic PPy composites, Wang et al. [23] have been synthesized uniform orange-like Fe$_3$O$_4$/PPy composite microspheres, the as-obtained Fe$_3$O$_4$/PPy microspheres showed strong adsorption capability with an adsorption capacity of about 209.2 mg·g^{-1}, and the adsorption capacity of Cr(VI) was not improved due to the lack of effective active sites. Moreover, Tuo et al. [24] synthesized Fe$_3$O$_4$/PPy composite nanofibers via in situ chemical polymerization, and Fe$_3$O$_4$/PPy nanofibers were employed to remove Cr(VI) and showed the strong adsorption capacity for Cr(VI) (312 mg·g^{-1}). These Fe$_3$O$_4$/PPy composites not only avoided the agglomeration of MNPs, but also enhanced the mechanical properties of PPy and exhibited high magnetic properties and low separation cost.

However, there are three challenges that limit the industrial application of magnetic PPy composites. The first is related to the low-adsorption capacity for Cr(VI), which will lead to the use of a large number of adsorbents in the treatment of wastewater containing heavy metal ions. The other is tedious synthesis processes of magnetic PPy composites. The last is loading amount of Fe$_3$O$_4$ on the adsorption capacity that has not been studied. Therefore, it is necessary to develop available technologies to prepare the magnetic PPy composites with excellent adsorption capacity.

Thus, we use a simple method for synthesis of the Fe$_3$O$_4$/PPy nanotubes using Py monomer as carbon and nitrogen source. MO was used as template, and Fe^{3+} initiated polymerization of Py monomer to form PPy nanotubes; subsequently, the remaining Fe^{3+} as iron source formed Fe$_3$O$_4$ in basic conditions. The effect of Fe^{3+} on the adsorption capacity was studied. Then, the structure and morphology of the synthesized Fe$_3$O$_4$/PPy nanotubes were characterized. Adsorption kinetics and isothermal adsorption of Fe$_3$O$_4$/PPy nanotubes will be studied. Meanwhile, the adsorption mechanism of Fe$_3$O$_4$/PPy nanotubes will be investigated to explore the high removal capability of Cr(VI) and easy separation of Fe$_3$O$_4$/PPy nanotubes.

2. Materials and Methods

2.1. Materials. Methyl orange (MO, Shanghai McLean Biochemical Technology Co., Ltd.), pyrrole monomer (Py, Aladdin Chemistry), hexahydrate and ferric trichloride (FeCl$_3$•6H$_2$O, Sinopharm Chemical Reagent Co., Ltd.), hydrochloric acid (HCl, Xilong Chemical Co, Ltd), K$_2$Cr$_2$O$_7$ (Li An Long Bo Hua Pharmaceutical chemical), and NH$_3$•H$_2$O (28 wt%, Sichuan Xiqiao Chemical). Ultrapure water was used in the whole experimental procedure.

2.2. Synthesis of Fe$_3$O$_4$/PPy Nanotubes. Fe$_3$O$_4$/PPy nanotubes were synthesized via the one-pot method (Figure 1). In a typical polymerization process, 0.98 g MO and a certain amount of FeCl$_3$•6H$_2$O were dissolved in 480 mL ultrapure water. Afterwards, 0.70 mL of Py was poured into the above mixture and slowly stirred for reaction 20 h at 25°C. 10 mL NH$_3$•H$_2$O were added, which reacts under the N$_2$ atmosphere for 4 h. Finally, the obtained green precipitates were washed repeatedly using ethanol and ultrapure water and then were dried at 60°C for 24 h. In order to study the effect of FeCl$_3$•6H$_2$O on morphology and property of Fe$_3$O$_4$/PPy nanotubes, Fe$_3$O$_4$/PPy nanotubes were synthesized by the mass of FeCl$_3$•6H$_2$O ranging between 4.50 g, 5.40 g, 6.75 g, 9.00 g, 13.50 g, and 27.00 g; the molar ratios of Py to Fe^{3+} (n (Py: Fe^{3+})) were 0.6, 0.5, 0.4, 0.3, 0.2, and 0.1; therefore the obtained products were named as S1, S2, S3, S4, S5, and S6, respectively.

2.3. Characterization of Fe$_3$O$_4$/PPy Nanotubes. The morphology of Fe$_3$O$_4$/PPy nanotubes was examined using scanning electron microscope (SEM), selected area electron diffraction (SAED), and transmission electron microscope (TEM). The surface functional group of Fe$_3$O$_4$/PPy nanotubes was characterized with Fourier transform infrared (FT-IR) spectrophotometer. The crystal structure of Fe$_3$O$_4$/PPy nanotubes was characterized by X-ray diffraction (XRD). The magnetization curves of Fe$_3$O$_4$/PPy nanotubes were measured with Vibration Sample Magnetometer (VSM). The thermal stability was performed by Thermal Analysis (TGA) in the range of 50°C to 800°C at N$_2$ atmosphere. The adsorption mechanism of the adsorbent was characterized with X-ray photoelectron spectroscopy (XPS).

2.4. Removal of Cr(VI). 1000 mg·L^{-1} stock solution of Cr(VI) was prepared by dissolving a certain amount of K$_2$Cr$_2$O$_7$ in
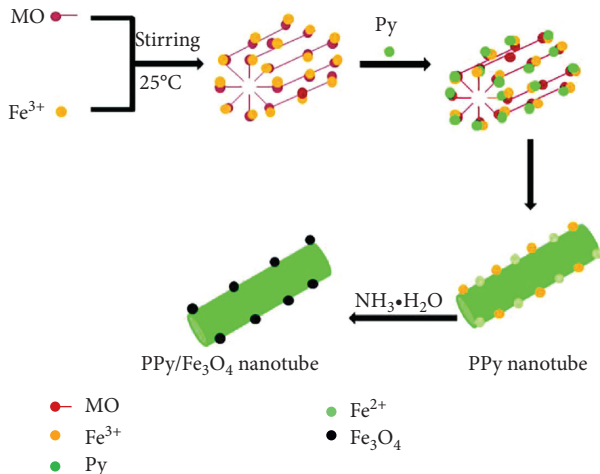
FIGURE 1: Schematic representation of the synthesis procedure of Fe_3O_4/PPy nanotubes.

ultrapure water. Different concentration of Cr(VI) was prepared by diluting stock solution. The standard curve of Cr(VI) was drawn at 540 nm with UV-visible spectrophotometer, according to the different concentrations of Cr(VI) standard solutions.

The adsorption experiment was carried out by keeping in contact 0.01 g of different adsorbents with 50 mL of 160 mg·L^{-1} Cr(VI) standard solution, and it was shaking in the oscillator at 25°C and 150 rpm for 24 h. In addition, the absorbance of Cr(VI) solution was determined at 540 nm with UV-visible spectrophotometer. The removal efficiency (R) and adsorption capacity (Q_e) of Cr(VI) were determined using the following equations:

$$R = \frac{(C_0 - C_e)}{C_0} \times 100\%, \tag{1}$$

$$Q_e = \frac{(C_0 - C_e)V}{m}, \tag{2}$$

where C_o and C_e represent the initial concentration of Cr(VI) and residual concentration of Cr(VI), respectively, V represents the initial volume of Cr(VI) solution, and m represents the mass of Fe_3O_4/PPy nanotubes.

The influence of reaction times on the adsorption property of Cr(VI) with Fe_3O_4/PPy nanotubes was discussed by varying the time from 0 to 24 h when the initial concentration of Cr(VI) was 160 mg·L^{-1}. Q_t was determined using

$$Q_t = \frac{C_0 - C_t V}{m}, \tag{3}$$

where Q_t and C_t are the adsorption capacity and the concentration of Cr(VI) at t, respectively.

2.5. Desorption Experiment of Fe_3O_4/PPy Nanotubes. 0.01 g of the S2 was added in a conical flask containing 50 mL of a 160 mg·L^{-1} Cr(VI) solution and allowed the interaction to proceed during 24 h. Then, the S2 was magnetically

separated by an external magnetic field, whereas the residual solution was collected for analysis using UV-Vis spectrophotometer at 540 nm. For the desorption experiment, Cr(VI) loaded adsorbent (S2) was exposed to 50 mL, 0.50 M NaOH solution in constant-temperature oscillator for 3 h at 150 rpm. Then, the S2 was washed by ultrapure water to neutralize and used in other adsorption/desorption cycles [20].

3. Results and Discussion

3.1. Morphology and Structure of Fe_3O_4/PPy Nanotubes. PPy nanotubes are explored by oxidative polymerization of Py monomer using various concentrations of $FeCl_3$ as oxidant and MO as a template. MO is electronegative in solution because of its hydrophilic edge group. Thus, Fe^{3+} can be attracted to the hydrophilic edge group of MO by electrostatic attraction and the formation of MO-$FeCl_3$ template. During oxidative polymerization of PPy, partial Fe^{3+} was reduced to Fe^{2+} by Py. Subsequently, Fe_3O_4/PPy nanotubes were formed using the remaining Fe^{3+} and reduced Fe^{2+} as iron source in the alkaline environment by coprecipitation approach. Figure 2 shows the XRD patterns of the Fe_3O_4 and various Fe_3O_4/PPy nanotubes. A wide peak appearing in the range of 20° to 30° is shown in all the Fe_3O_4/PPy nanotubes (Figures 2(a)–2(f)); this peak is mainly (002) diffraction peak for amorphous carbon, and the peak height decreases with the increasing of the Fe^{3+} concentration. For S1, other diffraction peaks except for (002) diffraction peaks are not observed in Figure 2(a). This is because Fe_3O_4 is difficult to form under a low concentration of Fe^{3+} and reduced Fe^{2+} in the reaction system, which has been calculated by chemical titration method. As the amount of Fe^{3+} increases, the six resolved different diffraction peaks appeared in the XRD of various Fe_3O_4/PPy nanotubes, correspond (220), (311), (400), (422), (511), and (440) diffraction peaks of Fe_3O_4 crystal (JCPDS card 74-0748), respectively, which indicates Fe_3O_4 are loaded upon PPy nanotubes. Besides, the peak intensity of Fe_3O_4 increased gradually, and the average sizes of Fe_3O_4 in nanocomposites calculated by Debye–Scherrer equation are between 9.20 nm and 15.40 nm, which is smaller than the average sizes of bare Fe_3O_4 nanoparticles (15.60 nm). This phenomenon suggests that Fe_3O_4 nanoparticles growing on the PPy nanotubes cause smaller grain sizes. Sun et al. [25] have reported similar phenomena.

The TEM images of PPy nanotubes are shown in Figure S1, and TEM images of various Fe_3O_4/PPy nanotubes, the SEM images, SAED pattern, and EDS profile of S2 are investigated as shown in Figure 3. The tubular structure has been formed when n(Py: Fe^{3+}) is 0.6, and particles agglomerated on the nanotubes are observed in Figure S1 (supporting information). PPy particles were formed before PPy nanotubes were formed, which is due to mechanism of coating growth for PPy nanotubes as the lack of oxidants. As the concentration of Fe^{3+} increases, integrated and smooth nanotubes were observed and the diameters of PPy nanotubes were decreased from 480 to 270 nm. The higher concentration of $FeCl_3$ leads to the diameter of MO-$FeCl_3$ micelle template decreases, which causes a smaller diameter
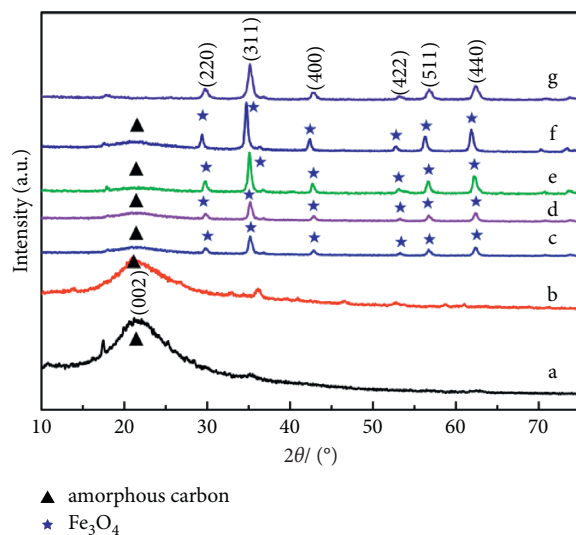
FIGURE 2: XRD pattern of S1 (a), S2 (b), S3 (c), S4 (d), S5 (e), S6 (f), and Fe_3O_4 (g).
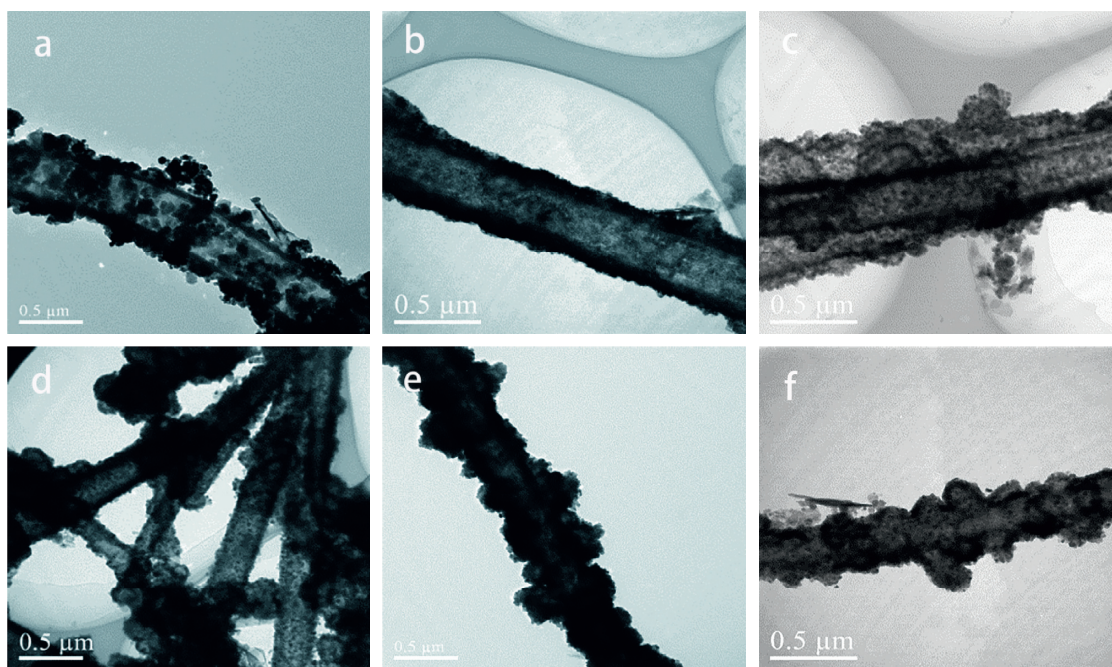

FIGURE 3: TEM pattern of S1 (a), S2 (b), S3 (c), S4 (d), S5 (e), and S6 (f).

of PPy nanotubes [26]. Also, the polymerization rate of Py monomer was quadratic with the concentration of $FeCl_3$, and the rapid polymerization rate of PPy may affect the formation of tubular morphology. In the presence of $NH_3 \bullet H_2O$, mass homogeneously nanoparticles were dispersed on PPy nanotubes as shown in Figures 3(a)–3(f). The SAED pattern of S2 (Figure 4(a)) exhibited diffraction rings of Fe_3O_4, which are consistent with that of XRD (Figure 2). Furthermore, the EDS profile of S2 (Figures 4(b)-4(c)) confirmed C, N, Fe, and O in the S2, and Fe elements are uniformly distributed on S2, which indicated that Fe_3O_4 is relatively uniformly dispersed on the PPy nanotubes.

The functional groups of Fe_3O_4/PPy nanotubes were investigated using FT-IR (Figure 5). For Fe_3O_4 (Figure 5(a)), the broad peaks centered around $3418\,cm^{-1}$, and the other peaks at $1619\,cm^{-1}$ and $1390\,cm^{-1}$ arise from the stretching vibrations and bending vibrations of O-H due to the residual moisture of Fe_3O_4. The crucial Fe-O stretching vibration in Fe_3O_4 appears at $583\,cm^{-1}$ [27]. IR spectrum of the PPy nanotubes (Figure 5(b)) and Fe_3O_4/PPy nanotubes (Figure 5(c)) indicates the presence of characteristic peaks Py, such as the characteristic adsorption peaks of Py rings ($1560\,cm^{-1}$ and $1465\,cm^{-1}$), the in-plane/out-of-plane C-H vibrations of Py ($1200\,cm^{-1}$, $930\,cm^{-1}$, and $775\,cm^{-1}$)
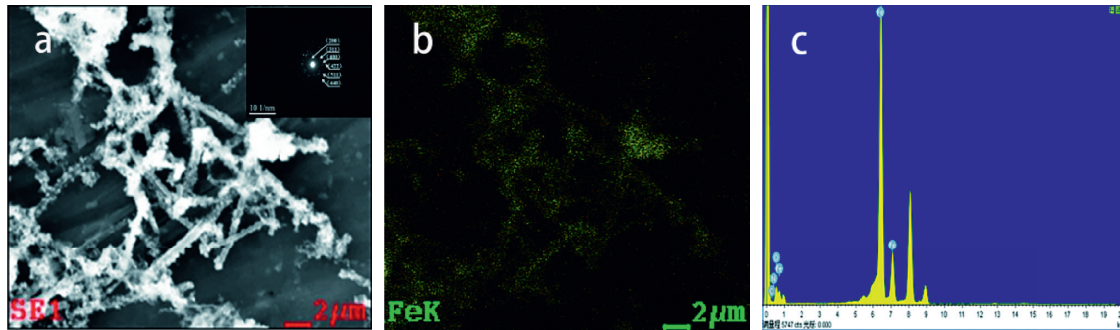
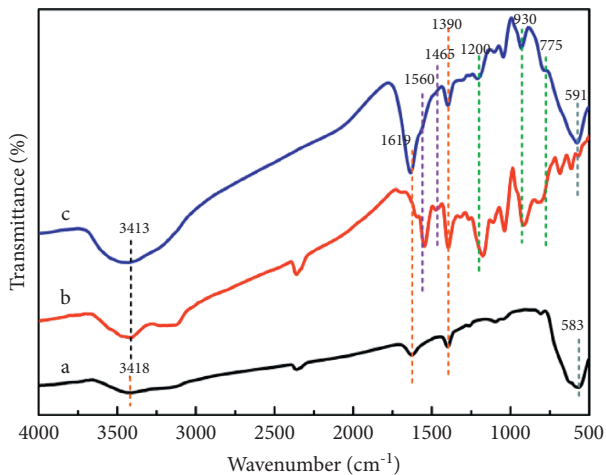FIGURE 4: SEM pattern (a), Fe distributing (b), and EDS profile (c) of S2.

FIGURE 5: Fourier infrared spectrum of Fe_3O_4 (a), PPy nanotubes (b), and Fe_3O_4/PPy nanotubes (c).

FIGURE 6: TGA curves of PPy nanotubes, S1, S2, S3, S4, S5, S6, and Fe_3O_4.

[28–30], and the stretching vibration of N-H ($3413 \, cm^{-1}$). Moreover, the Fe-O bond at $591 \, cm^{-1}$ was observed for Fe_3O_4/PPy nanotubes; it should be pointed out that the stretching vibration peak of Fe-O shifts to high wave numbers ($591 \, cm^{-1}$), which indicates that Fe_3O_4 is firmly bound to PPy nanotubes.

To test the thermal stability of the various Fe_3O_4/PPy nanotubes, TGA was carried out under the N_2 atmosphere from 50°C to 800°C (Figure 6). The TGA curves of the PPy nanotubes exhibit three steps in weight loss [31]. The weight loss processes of S1 and S2 were similar to PPy nanotubes because the content of Fe_3O_4 in the sample is shallow (5.21% and 7.91%). The first step of weight loss below 100°C is mainly due to the loss of bound water and residual moisture. The next step starts around 100°C to 290°C; the weight loss may correspond to the decomposition of MO and small organic molecules. The weight loss between 300°C and 800°C mainly relates to the decomposition and carbonization of PPy nanotubes. The S4, S5, and S6 show similar weight loss trends. A weight loss of 6% in the range of 50°C to 150°C is observed, which is attributed to desorption of gases and evaporation of residual moisture. As the temperature exceeds 150°C, the weight loss is related to the decomposition of MO and small organic molecules, and the weight loss is

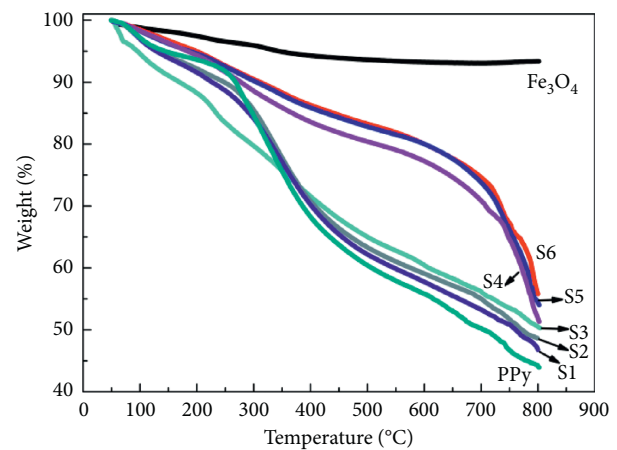enhanced with the increase of temperatures. A significant weight loss can be observed when the temperature exceeds 600°C, which is associated with the carbonization of PPy. From the thermograms, it has been seen that the rate of weight loss was much slower and residual quantity is much more with the increase in the concentration of Fe^{3+} in the Fe_3O_4/PPy nanotubes [32]. This indicated that the loading amounts of Fe_3O_4 in these PPy/Fe_3O_4 nanotubes increase (5.21 %–23.52%) and verify the XRD results.

3.2. Magnetic Behavior of Fe_3O_4/PPy Nanotubes. The hysteresis loops of Fe_3O_4/PPy nanotubes were measured with VSM to study the magnetic properties of various Fe_3O_4/PPy nanotubes. The magnetic hysteresis loops of Fe_3O_4/PPy nanotubes with various n(Py: Fe^{3+}) are shown in Figure 7. Various Fe_3O_4/PPy nanotubes and bare Fe_3O_4 are summarized in Table 1. In Figure 7, with the increase in concentration of Fe^{3+}, the saturation magnetizations (M_s) of Fe_3O_4/PPy nanotubes increased from 7.41 to 40.45 emu·g^{-1}, which may be due to the increase of Fe_3O_4 content during the reaction [33]. As shown in Table 1, the superparamagnetic behaviors of various Fe_3O_4/PPy nanotubes were confirmed by low M_r and coercivity H_c. Except for S1, Fe_3O_4/PPy nanotubes possess excellent magnetic properties,
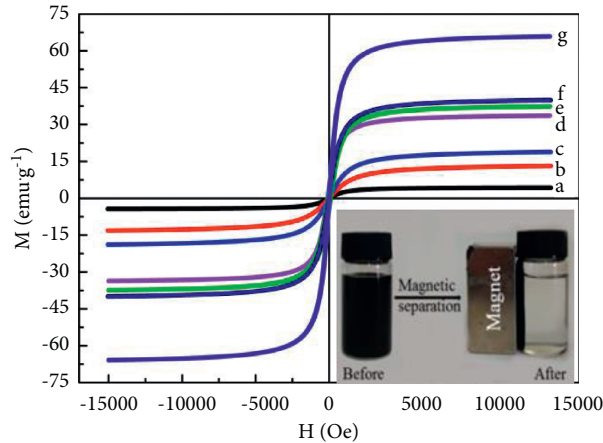
FIGURE 7: Magnetic hysteresis loops of S1 (a), S2 (b), S3 (c), S4 (d), S5 (e), S6 (f), and bare Fe_3O_4 (g).

TABLE 1: Magnetic properties of bare Fe_3O_4 and various Fe_3O_4/PPy nanotubes.

Sample name	M_s (emu·g^{-1})	M_r (emu·g^{-1})	M_r/M_s	H_c (Oe)
Fe_3O_4	65.87	2.81	0.04	16.24
S6	40.45	1.24	0.03	27.15
S5	37.39	1.12	0.03	18.45
S4	33.99	0.95	0.03	32.14
S3	19.71	0.47	0.02	16.01
S2	13.83	0.24	0.02	26.04
S1	7.41	0.17	0.02	21.04

which will provide an efficient way for separating Fe_3O_4/PPy nanotubes from solution.

3.3. Removal of Cr(VI) upon Fe_3O_4/PPy Nanotubes.

The adsorption property of Fe_3O_4, PPy, and various Fe_3O_4/PPy nanotubes for Cr(VI) from solution was investigated (Figure 8). Figure 8(a) shows the Q_e of Fe_3O_4, S2, and PPy nanotubes for Cr(VI) from solution. Q_e of Fe_3O_4/PPy nanotubes is significantly increased compared with bare Fe_3O_4. This is because the dispersion of Fe_3O_4 is improved after Fe_3O_4 is loaded on PPy nanotubes. Figure 8(b) shows the Q_e of various Fe_3O_4/PPy nanotubes for Cr(VI) from solution. Q_e increased with the increase in n(Py: Fe^{3+}) because the diameter of the Fe_3O_4/PPy nanotubes increases with the increase of n(Py: Fe^{3+}), and the more active sites were exposed, which cause enhanced the adsorption capacity.

The influence of adsorption times on the Q_t of various Fe_3O_4/PPy nanotubes was investigated, the initial concentration of Cr(VI) was 160 mg·L^{-1} at 25°C, and the adsorption time was varied from 0 h to 24 h (Figure 9). Q_t sharply increased up to an adsorption time of 2 h. Subsequently, the increase became relatively slow, and the adsorption equilibrium was reached at about 6 h. This adsorption behavior could be explained as follows. Generous active sites on Fe_3O_4/PPy nanotubes at the initial stage caused rapid adsorption of Cr(VI). However, the remaining active sites on the vacant surface sites were not readily occupied because of the increase in the inactivation of active sites and the repulsive force between the solute ions in the adsorbent and those in the liquid phase.

The effect of initial solution pH on removal of Cr(VI) by the PPy/Fe_3O_4 nanocomposite is shown in Figure 10. The concentration of Cr(VI) was 160 mg·L^{-1} at 25°C, and the solution pH was varied from 1 to 9. It is evident from Figure 10 that both the adsorption amount and removal rate of Cr(VI) decrease with the increase in the pH of the solution. This can be associated with the larger amount of OH$^-$ then present in the solution, which will compete with the CrO_4^{2-} for the same adsorption sites on the PPy surface.

The effect of the initial concentration of Cr(VI) from 20 mg/L to 200 mg/L on the adsorption properties was investigated at 25°C for 24 h. Figure 11 shows that the adsorption capacity (Q_e) increases rapidly with the increase in initial concentration when the initial concentration of Cr(VI) is lower than 120 mg/L. The increase of Q_e slows down gradually when the initial concentration of Cr(VI) is higher than 120 mg/L, and when the initial Cr(VI) concentration is increased to 160 mg/L, the adsorption equilibrium can be reached. The adsorption capacity is very low when the Cr(VI) concentration is low. This is because only a small amount of Cr(VI) reacts with the adsorption active site of adsorbent when the initial concentration is low. The increase of the initial concentration of Cr(VI) shows sharply increase of adsorption capacity. This increase in the adsorption capacity of Cr(VI) is the driving force for mass transfer becomes higher. The adsorption equilibrium process is eventually reached due to the adsorption active site of the adsorbent being occupied and steric hindrance. Moreover, it can be seen from Figure 11 that the maximum adsorption capacity of the Cr(VI) was 435.05 mg/g. The removal rate decreased as the initial concentration of Cr(VI) increased, and the maximum removal rate could reach 94.62% when the initial concentration of Cr(VI) was 20 mg/L.

3.4. Adsorption Kinetics.

To investigate the adsorption mechanism and describe the adsorption process of Cr(VI) on the surface of Fe_3O_4/PPy nanotubes, the ion adsorption

(a)

(b)

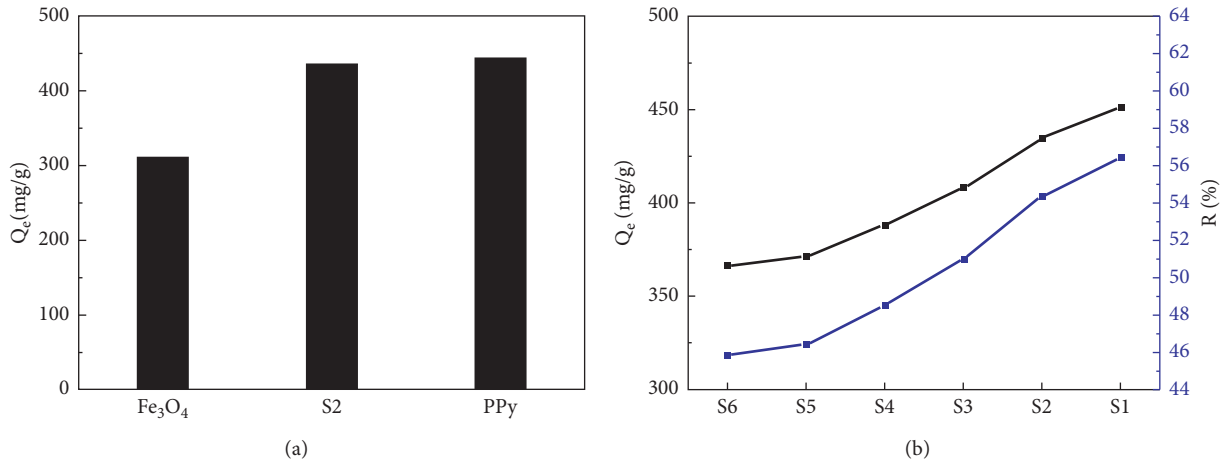FIGURE 8: Adsorption capacity of (a) Fe_3O_4, PPy, and S2 and (b) various Fe_3O_4/PPy nanotubes for Cr(VI).
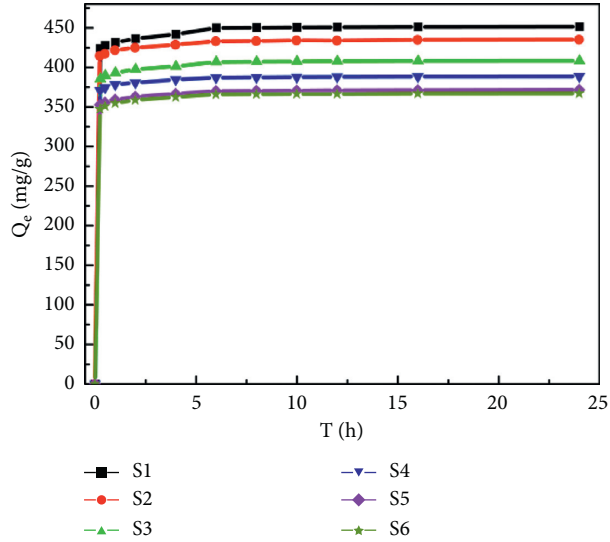

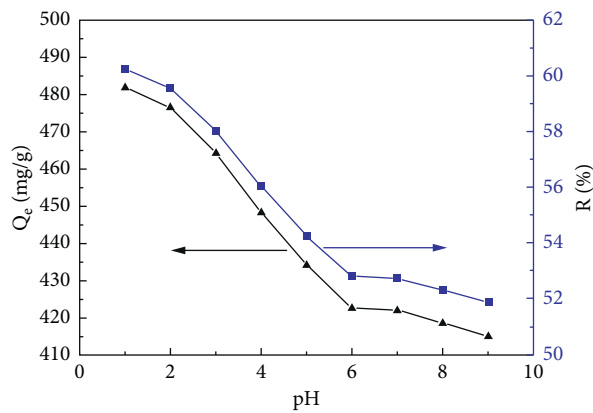FIGURE 9: Effects of contact times on adsorption capacity of Cr(VI) on various Fe_3O_4/PPy nanotubes.

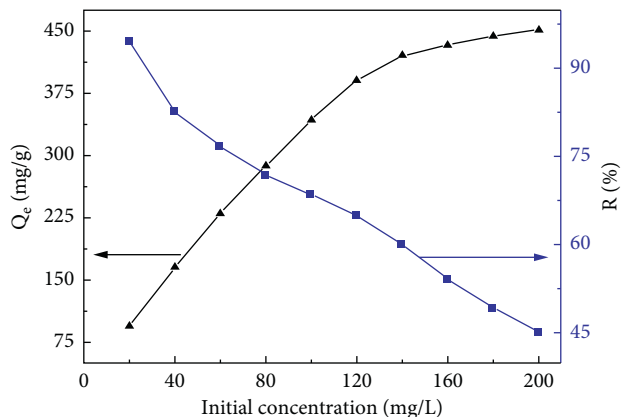FIGURE 10: Effect of pH on the removal of Cr(VI) by the PPy/Fe_3O_4 nanotubes (S2).

FIGURE 11: The effects of different initial concentrations of Cr(VI) on the removal of Cr(VI) by the PPy/Fe$_3$O$_4$ nanotubes (S2).

isotherms obtained in the adsorption experiments were fitted by pseudo-first-order kinetic model [34], pseudo-second-order kinetic model [35], and intraparticle diffusion kinetic model [36, 37]. This study on the adsorption kinetics of Cr(VI) can provide the basic data, theoretical reference, and technical support for Cr(VI) separation in the wastewater to use Fe$_3$O$_4$/PPy nanotubes, which has practical implications:

$$\text{pseudo-first-order model}: \ \log\left(Q_{e1} - Q_t\right) = \log Q_{e1} - \frac{k_1 t}{2.303},$$

$$\text{pseudo-second-order model}: \ \frac{t}{Q_t} = \frac{1}{k_2 Q_{e2}^2} + \frac{t}{Q_{e2}},$$

$$\text{intraparticle diffusion model}: Q_t = \text{ki}t^{1/2} + C, \tag{4}$$

where K_1 and K_2 are the equilibrium constants for kinetic models, Q_{e1} and Q_{e2} are the adsorption capacity of Cr(VI) on Fe$_3$O$_4$/PPy nanotubes at equilibrium, and K_i and C are the rate constant and the intercept of the intraparticle diffusion model.

The kinetic curves obtained by fitting the adsorption isotherms with kinetic models are shown in Figures 12(a) and 12(b), respectively. The corresponding rate constants of adsorption kinetic models and R^2 make a list in Table 2. It can be seen from Table 2, compared with the quasi-first-order kinetic model, the pseudo-second-order kinetic model well described the adsorption process of Cr(VI) on Fe$_3$O$_4$/ PPy nanotubes ($R_1^2 < R_2^2$), and Q_e calculated using the model was close to the experimental value. These results indicate that the rate control of Cr(VI) adsorption by Fe$_3$O$_4$/PPy nanotubes was controlled by a chemisorption mechanism, which mainly involved electron sharing and electron transfer between Fe$_3$O$_4$/PPy nanotubes and Cr ions.

The adsorption process was analyzed to confirm the mainly rate-controlling step with the intraparticle diffusion model. For Figure 12(c), the absorption process of Cr(VI) follows a multilinear diagram, and the results show that Cr(VI) was adsorbed on Fe$_3$O$_4$/PPy nanotubes in two steps. The first rapid step is surface or film diffusion; this is Cr(VI)

in solution moving towards the surface of the Fe$_3$O$_4$/PPy nanotubes. In this stage, large amounts of Cr(VI) were rapidly adsorbed onto the surface of the Fe$_3$O$_4$/PPy nanotubes; this was mainly physical adsorption. The second region is attributed to the intraparticle diffusion of Cr(VI) into the inner surface of Fe$_3$O$_4$/PPy nanotubes because a large amount of adsorbed Cr(VI) on the Fe$_3$O$_4$/PPy nanotubes need to be further diffused into the Fe$_3$O$_4$/PPy nanotubes pipeline, the same time, and Cr(VI) is combined with the adsorption active sites on the inner surface of the Fe$_3$O$_4$/PPy nanotubes, gradually adsorbed by the nanotube wall [38], and it involves physical adsorption and chemical adsorption. The adsorption parameters were obtained according to the slope and intercept as shown in Table 3. The results show that intraparticle diffusion was the main rate-limiting step in the integrated adsorption process of Cr(VI).

3.5. Adsorption Isotherms. We try to use the Langmuir [39], Freundlich [40], Temkin [41], and Dubinin and Radushkevich [42] isotherm adsorption models to describe the observed behavior of Cr(VI) adsorption towards S2. The related expressions are as follows:

$$\text{Langmuir}: \frac{C_e}{Q_e} = \frac{1}{K_L} + \frac{C_e}{Q_m},$$

$$R_L = \frac{1}{1 + K_L C_0},$$

$$\text{Freundlich}: \ln Q_e = \ln K_F + \frac{1}{n}\ln C_e,$$

$$\text{Temkin}: Q_e = \frac{RT}{b}\ln\left(K_T C_e\right),$$

$$Q_e = A + B \ln C_e,$$

$$A = \frac{RT}{b}\ln K_T, \tag{5}$$

$$B = \frac{RT}{b},$$

$$\text{Dubinin} - \text{Radushkevich}: \ln Q_e = \ln Q_m - \beta\varepsilon^2,$$

$$\varepsilon = RT \ln\left(1 + \frac{1}{C_e}\right),$$

$$E = \frac{1}{\sqrt{2\beta}},$$

where C_e and Q_m are equilibrium concentration and equilibrium adsorption capacity, K_L and K_F are Freundlich and Langmuir equilibrium constant, respectively, the value of R is 8.314, T is the reaction temperature, and K_T is the equilibrium binding constant.

The curves obtained by fitting the experimental data with isothermal adsorption models are shown in Figure 13. The relative parameters calculated from the four models
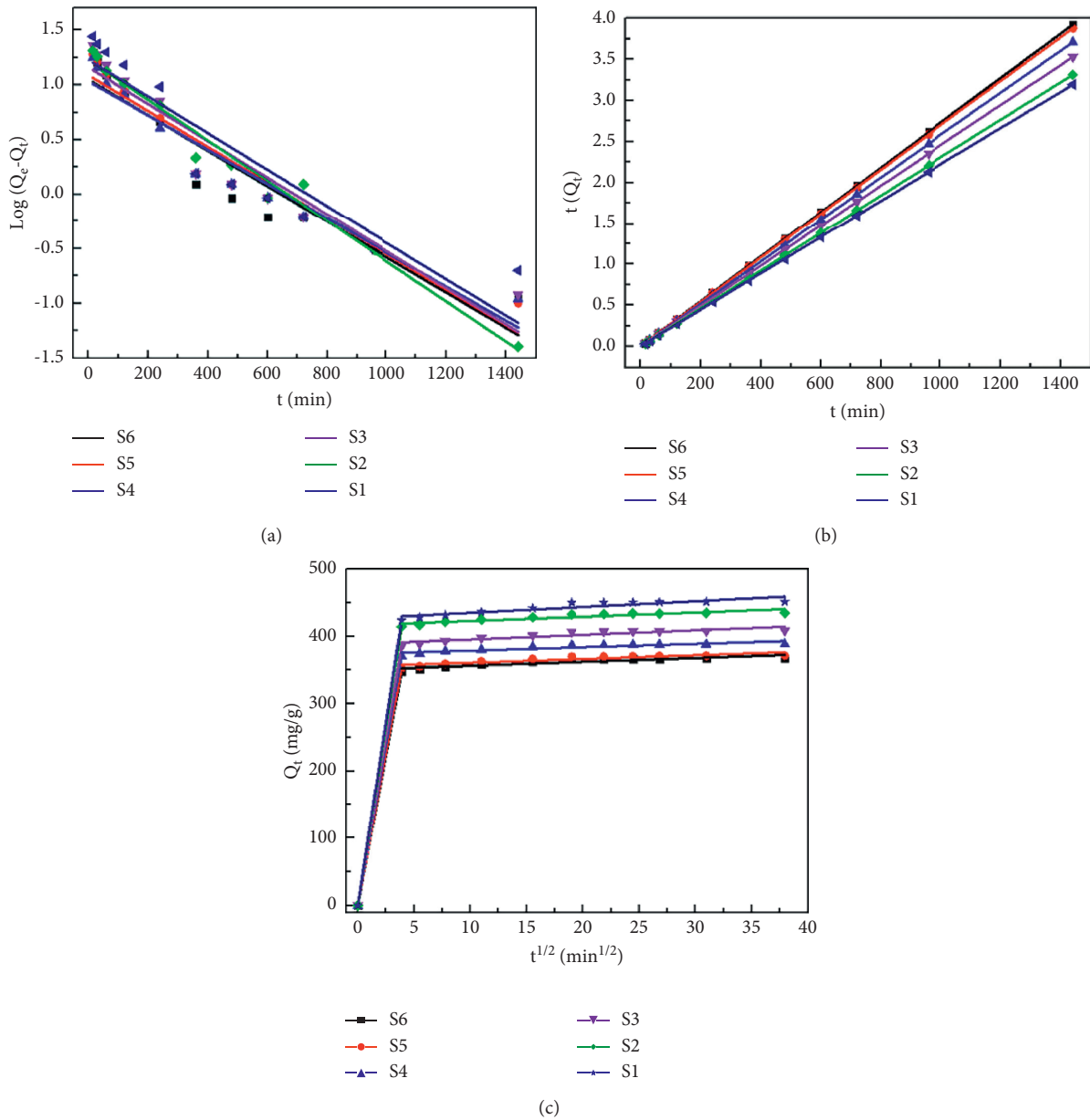
(a)

(b)

(c)

FIGURE 12: Pseudo-first-order kinetic (a), Pseudo-second-order kinetic (b), and (c) intraparticle diffusion models for adsorption of Cr(VI) onto various Fe_3O_4/PPy nanotubes.

TABLE 2: Pseudo-first-order and pseudo-second-order kinetic parameters for adsorption of Cr(VI) onto various Fe_3O_4/PPy nanotubes.

Sample name	Quasi-first order		Pseudo-second order		
	R_1^2	R_2^2	Q_e (mg·g^{-1})	K_2 (min^{-1})	Equation
S6	0.9505	0.9994	370.37	0.0014	$t/Q_t = 0.0027t + 0.0054$
S5	0.9703	0.9997	370.75	0.0013	$t/Q_t = 0.0027t + 0.0056$
S4	0.9701	0.9996	384.62	0.0015	$t/Q_t = 0.0026t + 0.0045$
S3	0.9598	0.9995	400.00	0.0011	$t/Q_t = 0.0025t + 0.0057$
S2	0.9899	0.9999	434.78	0.0010	$t/Q_t = 0.0023t + 0.0051$
S1	0.9328	0.9987	454.54	0.0008	$t/Q_t = 0.0022t + 0.0059$

(Langmuir, Freundlich, Temkin, and Dubinin–Radushkevich) are listed in Table 4. From the R^2 value, we can see that the Langmuir isotherm model can better describe our adsorption data, with R^2 values of 0.9918, and Q_{max} calculated with this model was close to the actual value. These results also show that the adsorption of Cr(VI) is

TABLE 3: Intraparticle diffusion model for adsorption of Cr(VI) onto various Fe_3O_4/PPy nanotubes.

Sample name	Rate constant	Value	R^2	Equation
S6	k_{i1} (mg·g^{-1}·min$^{-0.5}$)	89.67	1	$Q_t = 89.67t^{1/2}$
	k_{i2} (mg·g^{-1}·min$^{-0.5}$)	0.58	0.8826	$Q_t = 0.58t^{1/2} - 350.54$
S5	k_{i1} (mg·g^{-1}·min$^{-0.5}$)	91.04	1	$Q_t = 91.04t^{1/2} - 4 \times 20^{-14}$
	k_{i2} (mg·g^{-1}·min$^{-0.5}$)	0.56	0.8952	$Q_t = 0.56t^{1/2} - 355.03$
S4	k_{i1} (mg·g^{-1}·min$^{-0.5}$)	95.76	1	$Q_t = 95.76t^{1/2} - 4 \times 27^{-14}$
	k_{i2} (mg·g^{-1}·min$^{-0.5}$)	0.50	0.8881	$Q_t = 0.50t^{1/2} - 373.83$
S3	k_{i1} (mg·g^{-1}·min$^{-0.5}$)	99.52	1	$Q_t = 99.52t^{1/2} - 4 \times 25^{-14}$
	k_{i2} (mg·g^{-1}·min$^{-0.5}$)	0.69	0.8989	$Q_t = 0.69t^{1/2} - 388.36$
S2	k_{i1} (mg·g^{-1}·min$^{-0.5}$)	107.05	1	$Q_t = 107.05t^{1/2} - 4 \times 2^{-14}$
	k_{i2} (mg·g^{-1}·min$^{-0.5}$)	0.62	0.9091	$Q_t = 0.62t^{1/2} - 416.69$
S1	k_{i1} (mg·g^{-1}·min$^{-0.5}$)	109.45	1	$Q_t = 109.45t^{1/2} - 4 \times 10^{-14}$
	k_{i2} (mg·g^{-1}·min$^{-0.5}$)	0.87	0.9046	$Qt = 0.87t^{1/2} - 426.19$

(a)

(b)

(c)

(d)
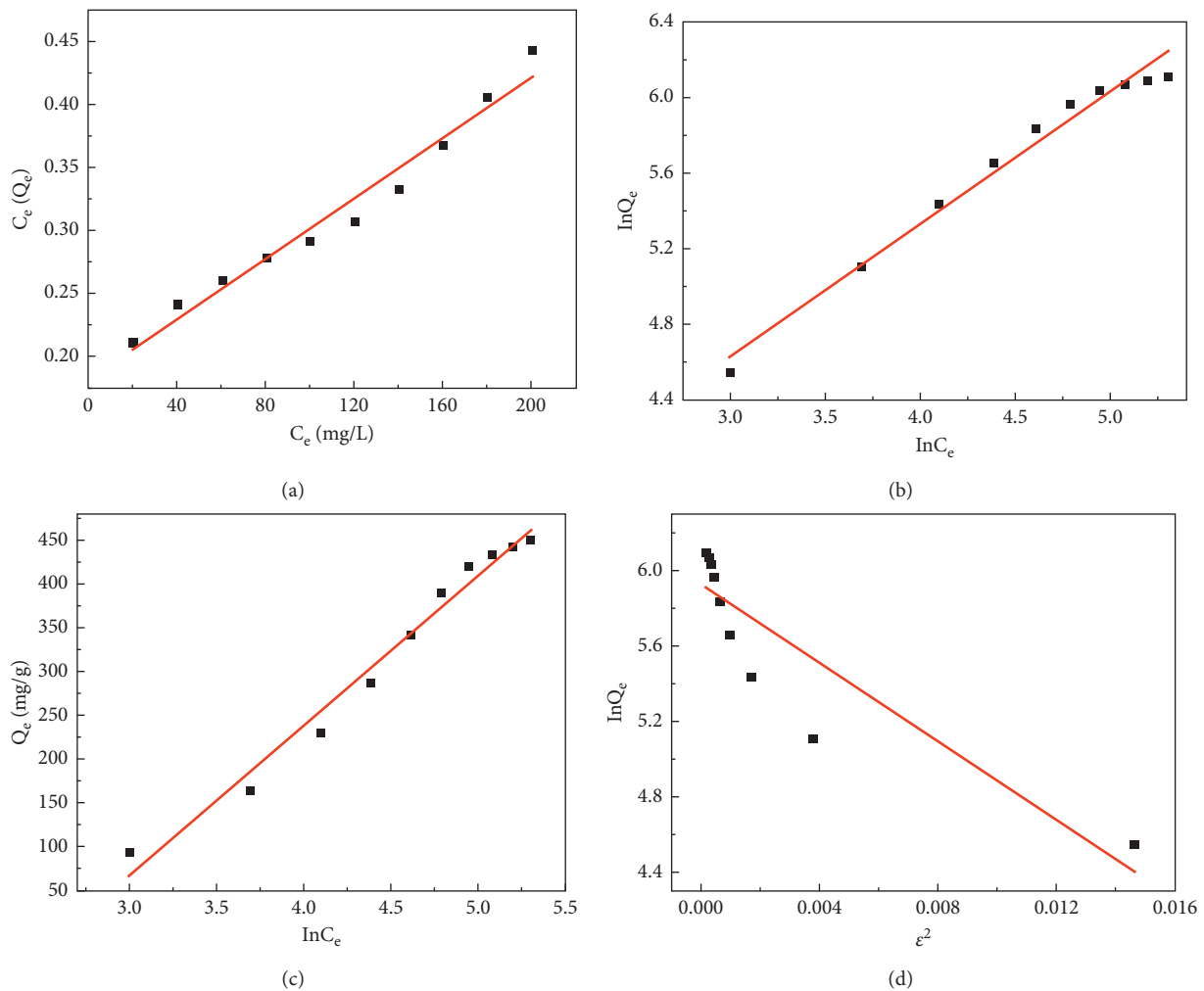
FIGURE 13: Cr(VI) adsorption on Fe_3O_4/PPy nanotubes described by (a) Langmuir, (b) Freundlich, (c) Temkin, and (d) Dubinin–Radushkevich isotherm adsorption models.

achieved by forming a monolayer on a uniform surface by a limited number of identical adsorption sites. In addition, the R_L values determined for the initial concentrations of Cr(VI) (20–200 mg·L^{-1}) were between 0 and 1, indicating that the system was favorable for adsorption.

A comparison of our work with other sorbents reported in literature has been registered, and the Q_m, adsorption conditions for removal of Cr(VI) and separation methods of different sorbents [10, 22, 43–49] are shown in Table 5. The results indicated that Fe_3O_4/PPy nanotubes prepared in this

TABLE 4: Adsorption isotherm model parameters for adsorption of Cr(VI) on S2.

Models	Constants	Value	R^2	Equation
Langmuir	Q_{max} (mg·g^{-1}) K_L (L·mg^{-1})	427.4646 0.0065	0.9918	$C_e/Q_e = 0.1823 + 0.0012C_e$
Freundlich	K_F (mg·g^{-1}) n (mg·L^{-1})	12.6606 1.4304	0.9896	$\ln Q_e = 2.5385 + 0.6991\ln C_e$
Temkin	K_T (L·g^{-1}) b (J·mol^{-1})	0.1142 14.4738	0.9891	$Q_e = 171.1723\ln C_e - 445.1788$
Dubinin–Radushkevich	Q_{max} (mg·g^{-1}) β (mol^2·kJ^{-2}) E (kJ·mol^{-1})	374.1288 103.9173 0.0693	0.8996	$\ln Q_e = 5.9246 - 103.9173\varepsilon^2$

TABLE 5: Comparison of Q_{max} of different sorbents for Cr(VI).

Adsorbents	Q_{max} (mg·g^{-1})	Conditions	Separation	Ref.
PPy/Fe$_3$O$_4$ nanocomposite	169.41	pH 2.0, 25°C	Magnetic	[10]
Fe$_3$O$_4$/PPy microsphere	209.21	pH 6.0, 25°C	Magnetic	[43]
Fe$_3$O$_4$/PPy nanofiber	202.83	pH 6.0, 25°C	Magnetic	[22]
PPy/Fe$_3$O$_4$ nanocomposite	230.17	pH 2.0, 25°C	Magnetic	[44]
PPy/γ-Fe$_2$O$_3$	209	pH 2.0, 25°C	Magnetic	[45]
Graphene/Fe$_3$O$_4$@PPy	348.4	pH 2.0, 25°C	Magnetic	[46]
PPy-Fe$_3$O$_4$/rGO	293.3	pH 3.0, 25°C	—	[47]
PPy-TP nanocomposite	31.64	pH 2.0, 45°C	—	[48]
PPy functionalized chitin	35.22	pH 4.8, 50°C	—	[49]
Fe$_3$O$_4$/PPy nanotubes	451.45	pH 6.0, 25°C	Magnetic	[Our work]

study have a good adsorption property of Cr(VI), which is a promising adsorbent for Cr(VI). Due to the large specific surface areas and more active adsorption sites in Fe$_3$O$_4$/PPy nanotubes, PPy nanotubes prevent the agglomeration of the Fe$_3$O$_4$ nanoparticles, which improves the adsorption efficiency of Fe$_3$O$_4$ nanoparticles for Cr(VI). In addition, the Fe$_3$O$_4$/PPy nanotubes can be easily separated from the wastewater under an external magnetic field and achieved its reuse. The excellent properties of Fe$_3$O$_4$/PPy nanotubes provide a strategy for adsorption of Cr(VI) from the wastewater.

To investigate the adsorption mechanism of Cr(VI) onto Fe$_3$O$_4$/PPy nanotubes, the XPS spectra before and after Fe$_3$O$_4$/PPy nanotubes adsorption are shown in Figure 14. As shown in Figure 14(a), after the adsorption of Cr(VI), the Cr2p peak was found on the nanotubes, which confirmed the existence of elemental Cr on the nanotubes. The high resolution spectrum of Cr2p is shown in Figure 14(b); there are two energy bands at 576.88 eV and 586.78 eV, which correspond to the Cr(2p3/2) and Cr(2p1/2) orbitals, respectively [10, 50]; the binding energies of 582.64 eV (2p3/2) and 590.36 eV (2p1/2) correspond to Cr(VI), and that of 588.82 eV (2p1/2) correspond to Cr(III). The binding energies of these peaks are similar to those reported by Bhaumik et al. [51]. After adsorption, the Cr(VI) and Cr(III) amounts are 34.53% and 65.47% in nanotubes, respectively, indicating that partial Cr(VI) was reduced by redox adsorption of S2. Figures 14(c)-14(d) reveal the three major energy peaks of the O1s at 529.88 eV, 531.08 eV, and 532.67 eV, corresponding to the oxygen of oxide O^{2-}, -C-O, and O-C=O, respectively [52]. The oxide (O^{2-}) group at 529.88 eV corresponds to the Fe-O group in the Fe$_3$O$_4$ crystal structure [53, 54]. The high-

resolution spectrum of Fe2p is shown in Figures 14(g)-14(h), which reveals the presence of two prominent bands at around 710.88 eV and 724.23 eV before adsorption, corresponding to Fe2p3/2 and Fe2p1/2 in Fe$_3$O$_4$, respectively [55]. After adsorption, Fe2p and the O^{2-} groups in O1s show a slight decrease in area, which may be due to the separation or oxidation of a small amount of Fe$_3$O$_4$ nanoparticle on S2 surface, indicating that PPy can protect the Fe$_3$O$_4$ nanoparticles and improve their stability. The XPS spectra of N1s (Figures 14(e)-14(f) show obvious changes. Before adsorption, three peaks appeared at 399.64 eV, 399.90 eV, and 402.88 eV, which can be assigned to quinoid imine (=N-), imino group (-NH-), and positively charged nitrogen (-NH$^+$). After adsorption, the area of the peak at 399.64 eV and 402.88 eV decreases. The ion exchange could happen between Cr(VI) and the quinoid imine (=N-), and redox adsorption can happen between Cr(VI) and nitrogen with positive charge (-NH$^+$) [56]; the partly Cr(VI) was reduced to Cr(III).

3.6. Reusability of Fe$_3$O$_4$/PPy Nanotubes.
The reusability and regeneration ability of adsorbents are very important in practical applications. In this work, the solvent regeneration method was used to recover the adsorbent, which had the advantages of simple operation, high efficiency, no secondary pollution, and low cost [26]. Cr(VI) was removed from chromium loaded S2 adsorbent (0.01 g) which was conducted using 50 mL of 0.5 M NaOH. Figure 14(i) shows the cycle stability of S2 adsorption of Cr(VI). The results show that about 90% removal efficiency of Cr(VI) could be retained after five cycles. This indicates that the Fe$_3$O$_4$/PPy nanotubes have good reusability.
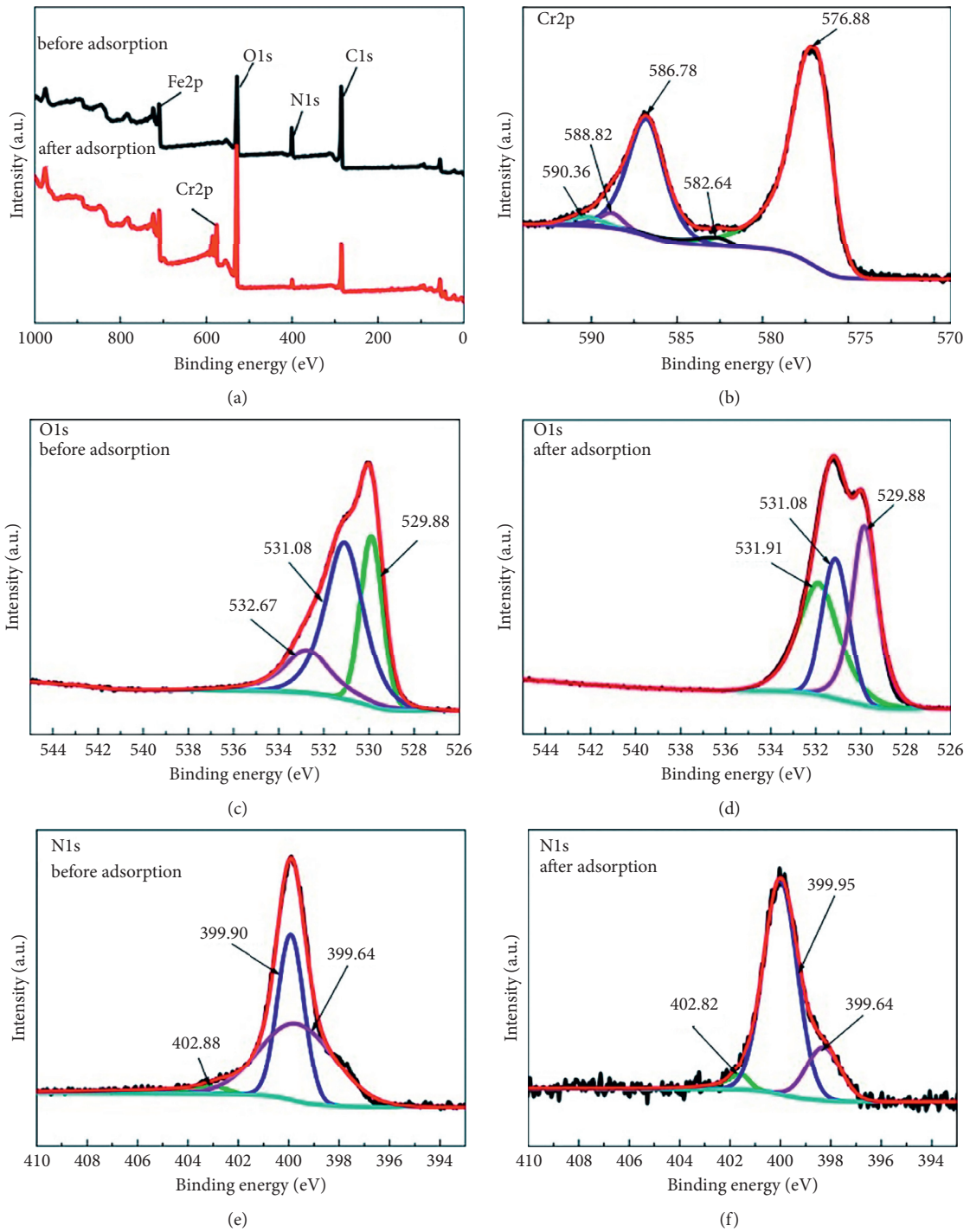
(a)

(b)

(c)

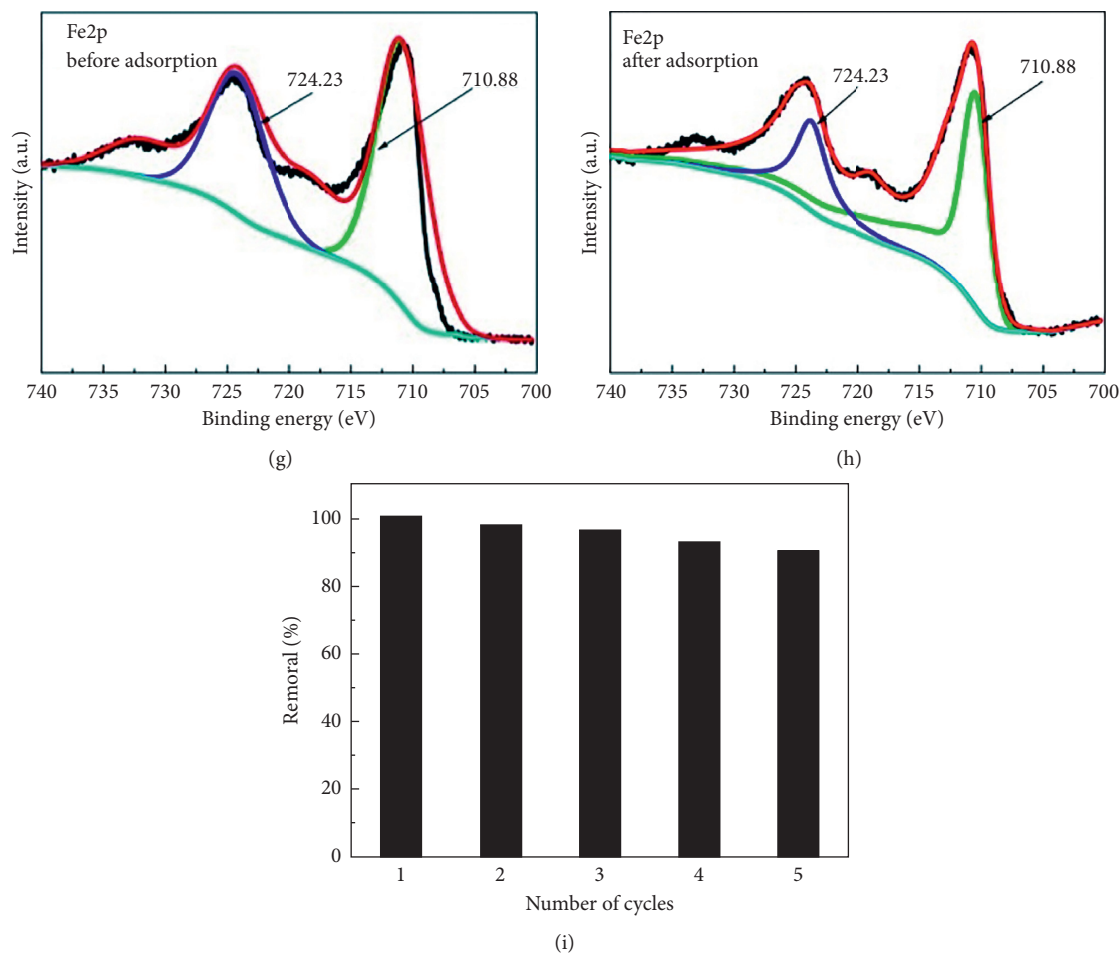(d)

(e)

(f)

Figure 14: Continued.

(g)

(h)

(i)

FIGURE 14: XPS spectra (a) of Fe_3O_4/PPy nanotubes before and after adsorption of Cr(VI), high-resolution spectra of Cr2p (b) after adsorption of Cr(VI). XPS spectra of O1 s(c, d), N1s (e, f), and Fe2p (g, h) for Fe_3O_4/PPy nanotubes before and after adsorption of Cr(VI), and (i) adsorption and desorption cycles of Fe_3O_4/PPy nanotubes.

4. Conclusions

The Fe_3O_4/PPy nanotubes using Py monomer as carbon and nitrogen source, MO as a template, and $FeCl_3 \cdot 6H_2O$ as initiator and iron source were synthesized by one-pot approach. The diameter of Fe_3O_4/PPy nanotubes was decreased with the increasing of the Fe^{3+} concentration. The Fe_3O_4 nanoparticles are uniformly distributed on the PPy nanotubes and the size of Fe_3O_4 with nanocomposites are all smaller than the average sizes of bare Fe_3O_4. The Fe_3O_4/PPy nanotubes show superparamagnetic properties and can be magnetically separated under external magnetic field. Moreover, the magnetic adsorbent was used to remove Cr(VI). The adsorption capacity of Fe_3O_4/PPy nanotubes was significantly increased compared with bare Fe_3O_4, and the adsorption capacity of Fe_3O_4/PPy nanotubes was decreased with the increasing of the Fe^{3+} concentration and adsorption capacity from 367.16 to 451.45 mg·g^{-1} for Cr(VI) in aqueous solution. The adsorption kinetics data could be well fitted with the pseudo-second-order kinetic model, indicating that the adsorption process was controlled by a physical and chemical adsorption mechanism. The adsorption isotherm of Cr(VI) on Fe_3O_4/PPy nanotubes was highly consistent with the Langmuir isotherm adsorption model, suggesting that Cr(VI) adsorption was single-layer adsorption and a favorable process. The XPS study also showed that the ion exchange and reduction were the adsorption mechanism for removal of Cr(VI) by the Fe_3O_4/PPy nanotubes. The Fe_3O_4/PPy nanotubes could be recyclable, retaining the removal efficiency at about 90% after five cycles, indicating the potential of the adsorbent to remove Cr(VI) from wastewater.

Data Availability

The data used to support the findings of this study are included within the article.

Conflicts of Interest

The authors declare that they have no conflicts of interest.

Acknowledgments

Supplementary Materials

Fig. S1 was provided in the Supplementary Material for comprehensive image analysis. (*Supplementary Materials*)

References

[1] M. K. Aroua, F. M. Zuki, and N. M. Sulaiman, "Removal of chromium ions from aqueous solutions by polymer-enhanced ultrafiltration," *Journal of Hazardous Materials*, vol. 147, no. 3, pp. 752–758, 2007.

[2] N. N. Thien, L. S. Ying, S. S. Chen et al., "Preparation of Zn-doped biochar from sewage sludge for chromium ion removal," *Journal of Nanoscience and Nanotechnology*, vol. 18, no. 8, pp. 5520–5527, 2018.

[3] A. Katz and S. Harry, "The toxicology of chromium with respect to its chemical speciation: a review," *Journal of Applied Toxicology*, vol. 13, no. 3, pp. 217–224, 1993.

[4] A. M. Yusof and N. A. Malek, "Removal of Cr(VI) and As(V) from aqueous solutions by HDTMA-modified zeolite Y," *Journal of Hazardous Materials*, vol. 162, no. 15, pp. 1019–1024, 2009.

[5] W.-J. Zhang, B.-B. Zhang, X.-Y. Du, Y.-L. Wang, Y.-L. Fei, and Y.-Y. Shen, "Synthesis of N-doped magnetic mesoporous carbon composites for adsorption of Ag(I) in aqueous solution," *Journal of Nanoscience and Nanotechnology*, vol. 21, no. 3, pp. 1462–1473, 2021.

[6] B. Hu and H. Luo, "Adsorption of hexavalent chromium onto montmorillonite modified with hydroxyaluminum and cetyltrimethylammonium bromide," *Applied Surface Science*, vol. 257, no. 3, pp. 769–775, 2010.

[7] J. Hu, G. Chen, and I Lo, "Removal and recovery of Cr(VI) from wastewater by maghemite nanoparticles," *Water Research*, vol. 39, no. 18, pp. 4528–4536, 2005.

[8] A. F. Ngomsik, A. Bee, and M. Draye, "Magnetic nano- and microparticles for metal removal and environmental applications: a review," *Comptes Rendus Chimie*, vol. 8, no. 6-7, pp. 963–970, 2005.

[9] L. Li, M. Fan, R. C. Brown et al., "Synthesis, properties, and environmental applications of nanoscale iron-based materials: a review," *Critical Reviews in Environmental Science and Technology*, vol. 36, no. 5, pp. 405–431, 2006.

[10] G. Y. Mao and F. X. Bu, "Synthesis, characterization and adsorption properties of magnetic γ-Fe$_2$O$_3$/C nanocomposite," *Journal of Nanoscience and Nanotechnology*, vol. 8, no. 15, pp. 5924–5932, 2015.

[11] Y. G. Guo, J. S. Hu, and L. J. Wan, "Nanostructured materials for electrochemical energy conversion and storage devices," *Advanced Materials*, vol. 20, no. 23, pp. 2878–2887, 2008.

[12] Z. Wang, D. Luan, S. Madhavi, Y. Hu, and X. W. Lou, "Assembling carbon-coated α-Fe2O3hollow nanohorns on the CNT backbone for superior lithium storage capability," *Energy & Environmental Science*, vol. 5, no. 1, pp. 5252–5256, 2012.

[13] B. Tural, N. Özkan, and M. Volkan, "Preparation and characterization of polymer coated superparamagnetic magnetite nanoparticle agglomerates," *Journal of Physics and Chemistry of Solids*, vol. 70, no. 5, pp. 860–866, 2009.

[14] J. Meng, J. Bu, C. Deng, and X. Zhang, "Preparation of polypyrrole-coated magnetic particles for micro solid-phase extraction of phthalates in water by gas chromatography-mass spectrometry analysis," *Journal of Chromatography A*, vol. 1218, no. 12, pp. 1585–1591, 2011.

[15] C. Weidlich, K.-M. Mangold, and K. Jüttner, "Conducting polymers as ion-exchangers for water purification," *Electrochimica Acta*, vol. 47, no. 5, pp. 741–745, 2001.

[16] C. Zhou, H. Zhu, Q. Wang, and J. X. Wang, "Adsorption of mercury(ii) with an Fe$_3$O$_4$ magnetic polypyrrole-graphene oxide nanocomposite," *RSC Advances*, vol. 7, no. 579, pp. 18466–18479, 2017.

[17] J. J. Luo and Q. F. Lu, "Controllable preparation and heavy-metal-ion adsorption of lignosulfonate -polypyrrole composite nanosorbent," *Polymer Composites*, vol. 36, no. 5, p. 1546, 2011.

[18] Y. Lei, X. Qian, J. Shen, and X. An, "Integrated reductive/adsorptive detoxification of Cr(VI)-Contaminated water by polypyrrole/cellulose fiber composite," *Industrial & Engineering Chemistry Research*, vol. 51, no. 31, pp. 10408–10415, 2012.

[19] T. Yao, T. Cui, J. Wu, Q. Chen, S. Lu, and K. Sun, "Preparation of hierarchical porous polypyrrole nanoclusters and their application for removal of Cr(vi) ions in aqueous solution," *Polymer Chemistry*, vol. 2, no. 12, pp. 2893–2899, 2011.

[20] A. E. Chávez-Guajardo, J. C. Medina-Llamas, L. Maqueira, C. A. S. Andrade, K. G. B. Alves, and C. P. de Melo, "Efficient removal of Cr (VI) and Cu (II) ions from aqueous media by use of polypyrrole/maghemite and polyaniline/maghemite magnetic nanocomposites," *Chemical Engineering Journal*, vol. 281, no. 1, pp. 826–836, 2015.

[21] P. Xiangqian, Z. Wei, G. Ligang, J. Haihui, W. Yang, and Z. Lichun, "Dedoped Fe$_3$O$_4$/PPy nanocomposite with high anti-interfering ability for effective separation of Ag(I) from mixed metal-ion solution," *Chemical Engineering Journal*, vol. 280, pp. 197–205, 2015.

[22] B. Madhumita and M. Arjun, "Enhanced removal of Cr(VI) from aqueous solution using polypyrrole/Fe$_3$O$_4$ magnetic nanocomposite," *Journal of Hazardous Materials*, vol. 190, pp. 381–390, 2011.

[23] Y. Wang, B. Zou, T. Gao, X. Wu, S. Lou, and S. Zhou, "Synthesis of orange-like Fe3O4/PPy composite microspheres and their excellent Cr(vi) ion removal properties," *Journal of Materials Chemistry*, vol. 22, no. 18, pp. 9034–9040, 2012.

[24] X. Tuo, B. Li, X. Yu et al., "Facile synthesis of magnetic polypyrrole composite nanofibers and their application in Cr(VI) removal," *Polymer Composites*, vol. 39, no. 5, pp. 1507–1513, 2018.

[25] X. Sun, C. Zheng, F. Zhang et al., "Size-controlled synthesis of magnetite (Fe$_3$O$_4$) nanoparticles coated with glucose and gluconic acid from a single Fe(III) precursor by a sucrose bifunctional hydrothermal method," *Journal of Physical Chemistry C*, vol. 113, no. 36, pp. 16002–16008, 2009.

[26] J. C. Thuebkenont, J. L. Gabelle, and M. F. Planche, "Polypyrrole over-oxidation during its chemical synthesis," *Synthetic Metals*, vol. 66, no. 3, pp. 243–247, 1994.

[27] L. Gai, X. Han, Y. Hou, J. Chen, H. Jiang, and X. Chen, "Surfactant-free synthesis of Fe3O4@PANI and Fe3O4@PPy microspheres as adsorbents for isolation of PCR-ready DNA," *Dalton Transactions*, vol. 42, no. 5, pp. 1820–1826, 2013.

[28] G. Qiu, Q. Wang, and M. Nie, "Polypyrrole-Fe3O4 magnetic nanocomposite prepared by ultrasonic irradiation," *Macromolecular Materials and Engineering*, vol. 291, no. 1, pp. 68–74, 2006.

[29] H. P. de Oliveira, C. A. S. Andrade, and C. P. de Melo, "Electrical impedance spectroscopy investigation of surfactant-magnetite-polypyrrole particles," *Journal of Colloid and Interface Science*, vol. 319, no. 2, pp. 441–449, 2008.

[30] J. G. Deng, Y. X. Peng, C. L. He, and X. P. Long, "Magnetic and conducting Fe_3O_4-polypyrrole nanoparticles with core-shell structure," *Polymer International*, vol. 52, no. 14, pp. 1182–1187, 2003.

[31] S. Shang, X. Yang, and X. Tao, "Easy synthesis of carbon nanotubes with polypyrrole nanotubes as the carbon precursor," *Polymer*, vol. 50, no. 13, pp. 2815–2818, 2009.

[32] J. Upadhyay and A. Kumar, "Structural, thermal and dielectric studies of polypyrrole nanotubes synthesized by reactive self degrade template method," *Materials Science and Engineering: B*, vol. 178, no. 15, pp. 982–989, 2013.

[33] Y. K. Sun, D. Y. Li, H. Yang, and X. Z. Guo, "Fabrication of Fe_3O_4@polydopamine@polyamido-amine core–shell nanocomposites and its application for Cu (II) adsorption," *New Journal of Chemistry*, vol. 9, no. 16, pp. 195–197, 2018.

[34] Y. S. Ho and G. McKay, "The sorption of lead(II) ions on peat," *Water Research*, vol. 33, no. 2, pp. 578–584, 1999.

[35] N. Hamadi, X. D. Chen, and M. M. Farid, "Adsorption kinetics for the removal of chromium(VI) from aqueous solution by adsorbents derived from used tyres and sawdust," *Chemical Engineering Journal*, vol. 84, no. 2, pp. 95–105, 2001.

[36] W. J. Weber and J. C. Morris, "Removal of biologically resistant pollutant from waste waters by adsorption," *Advances in Water Pollution Research*, vol. 2, pp. 231–266, 1964.

[37] W. J. Weber and J. C. Morris, "Kinetics of adsorption on carbon from solution," *Journal of the Sanitary Engineering Division*, vol. 89, no. 2, pp. 31–59, 1963.

[38] R. J. Li, "Adsorptive removal of Hg (II), Cr (VI) and Pb (II) ions from aqueous solutions using nitrogen-containing conductive polymer composites," *Dalian University of Technology*, pp. 51-52, 2016.

[39] I. Langmuir, "The constitution and fundamental properties of solids and liquids. part I. solids," *Journal of the American Chemical Society*, vol. 38, no. 11, pp. 2221–2295, 1916.

[40] H. Freundlich, "Over the adsorption in solution," *Journal of Physical Chemistry*, vol. 57, pp. 385–471, 1906.

[41] S. Z. Roginsky and Y. B. Zeldovich, "Die katalische oxidation von kohlenmonoxyd auf mangan-dioxyd," *Acta Physiochimica URSS*, vol. 1, pp. 554–594, 1934.

[42] M. M. Dubinin and L. V. Radushkevich, "Equation of the characteristic curve of the activated charcoal," *Chemisches Zentralblatt*, vol. 1, pp. 875–890, 1947.

[43] J. Liu and M. Wan, "Composites of polypyrrole with conducting and ferromagnetic behaviors," *Journal of Polymer Science Part A: Polymer Chemistry*, vol. 38, no. 15, pp. 2734–2739, 2000.

[44] M. Bhaumik, M. Arjun, S. Katlego, and O. Maurice S., "Chromium (VI) removal from water using fixed bed column of polypyrrole/Fe3O4 nanocomposite," *Separation and Purifcation Technology*, vol. 110, no. 7, pp. 11–19, 2013.

[45] A. C. Alicia, C. M. Juan, and M. Luis, "Use of magnetic and fluorescent polystyrene/tetraphenyl porphyrin/maghemite nanocomposites for the photoinactivation of pathogenic bacteria," *Reactive and Functional Polymers*, vol. 96, pp. 39–43, 2015.

[46] A. M. Muliwa, T. Y. Leswifi, M. S. Onyango, and A. Maity, "Magnetic adsorption separation (MAS) process: an alternative method of extracting Cr(VI) from aqueous solution using polypyrrole coated Fe 3 O 4 nanocomposites," *Separation and Purification Technology*, vol. 158, no. 28, pp. 250–258, 2016.

[47] H. Wang, X. Yuan, Y. Wu et al., "Facile synthesis of polypyrrole decorated reduced graphene oxide-Fe3O4 magnetic composites and its application for the Cr(VI) removal," *Chemical Engineering Journal*, vol. 262, no. 15, pp. 597–606, 2015.

[48] R. Rifaqat and K. Ali, "Removal of carcinogenic hexavalent chromium from aqueous solutions using newly synthesized and characterized polypyrrole-titanium (IV) phosphate nanocornpo-site," *Chemical Engineering Journal*, vol. 280, no. 15, pp. 494–504, 2015.

[49] K. Rathinam and M. Sankaran, "Synthesis, characterization and Cr (VI) uptake studies of polypyrrole functionalized chitin," *Synthetic Metals*, vol. 198, pp. 181–187, 2014.

[50] H. Gu, S. B. Rapole, J. Sharma et al., "Magnetic polyaniline nanocomposites toward toxic hexavalent chromium removal," *RSC Advances*, vol. 2, no. 29, pp. 11007–11018, 2012.

[51] M. Bhaumik, A. Maity, V. V. Srinivasu, and M. S. Onyango, "Removal of hexavalent chromium from aqueous solution using polypyrrole-polyaniline nanofibers," *Chemical Engineering Journal*, vol. 181-182, no. 1, pp. 323–333, 2012.

[52] K. Song, Y. Lee, M. R. Jo, and K. M. Nam, "Comprehensive design of carbon-encap sulated Fe_3O_4 nanocrystals and their lithium storage properties," *Nanotechnology*, vol. 23, no. 11, Article ID 505401, 2012.

[53] X. C. Zhao, D. S. Su, R. Sylvia et al., "Reactivity of mesoporous carbon against water-an in-situ XPS study," *Carbon October*, vol. 77, pp. 175–183, 2014.

[54] L. S. Fang, Y. M. Zheng, and C. J. Paul, "Organic arsenic adsorption onto a magnetic sorbent," *Langmuir*, vol. 25, no. 9, pp. 4973–4978, 2009.

[55] W. Chen, S. Li, C. Chen, and L. Yan, "Self-assembly and embedding of nanoparticles by in situ reduced graphene for preparation of a 3D graphene/nanoparticle aerogel," *Advanced Materials*, vol. 23, no. 4, pp. 5679–5683, 2011.

[56] W. H. Sun, W. B. Zhang, and H. L. Li, "Insight into the synergistic effect on adsorption for Cr (VI) by a polypyrrole-based composite," *RSC Advances*, vol. 10, no. 8, pp. 87–90, 2020.